Quantifying the contribution of anthropogenic influence to the East Asian winter monsoon in 1960–2012

Xin Hao*[1,2], Shengping He[4,1], Huijun Wang[1,2,3], Tingting Han[1,2]

[1] Collaborative Innovation Center on Forecast and Evaluation of Meteorological Disasters/Key Laboratory of Meteorological Disaster, Ministry of Education, Nanjing University for Information Science and Technology, Nanjing 210044, China

[2] Nansen-Zhu International Research Centre, Institute of Atmospheric Physics, Chinese Academy of Sciences, Beijing 100029, China

[3] Climate Change Research Center, Chinese Academy of Sciences, Beijing100029, China

[4] Geophysical Institute, University of Bergen and Bjerknes Centre for Climate Research, Bergen 0025, Norway

Corresponding author: Xin Hao, haoxlike91@163.com

Abstract

The East Asian winter monsoon (EAWM) can be greatly influenced by many factors that can be classified as anthropogenic forcing and natural forcing. Here we explore the contribution of anthropogenic influence to the change in the EAWM over the past decades. Under all forcings observed during 1960–2013 (All-Hist run), the atmospheric general circulation model is able to reproduce the climatology and variability of the EAWM-related surface air temperature and 500 hPa geopotential height, and shows a statistically significant decreasing EAWM intensity with a trend coefficient of ~ -0.04 yr^{-1} which is close to the observed trend. By contrast, the simulation, which is driven by the same forcing as All-Hist run but with the anthropogenic contribution to them removed, shows no decreasing trend in the EAWM intensity. By comparing the simulations under two different forcing scenarios, we further reveal that the responses of the EAWM to the anthropogenic forcing include a rise of $0.6℃$ in surface air temperature over the East Asia as well as weakening of the East Asia trough, which may result from the poleward expansion and intensification of the East Asian jet forced by the change of temperature gradient in the

troposphere. Additionally, compared with the simulation without anthropogenic forcing, the frequency of strong (weak) EAWM occurrence is reduced (increased) by 45% (from 0 to 10/7). These results indicate that the weakening of the EAWM during 1960–2013 may be mainly attributed to the anthropogenic influence.

Key words: anthropogenic influence, East Asian winter monsoon, contribution

1. Introduction

The East Asian winter monsoon (EAWM) is one of the most dominant climate systems in East Asia. It greatly affects the disastrous winter weather such as cold waves, snowstorms, air pollutions, and spring duststorms (Li et al., 2016; Li and Wang, 2013; Wang et al., 2009; Zhou et al., 2009; Chang et al., 2006). Prominent circulation components from surface to the upper troposphere associated with temperature condition during the boreal winter are dynamically linked to the EAWM. At surface, the EAWM contains the cold Siberian high dominated over the East Asian continent and the warm Aleutian low located in the high-latitude North Pacific, which accompanies with prevailing northwesterly winds in the low-level troposphere (He and Wang, 2013; Wang and Jiang, 2004; Gong et al., 2001; Guo 1994; Lau and Li, 1984). At 500 hPa locates the East Asian trough which determines the outbreak and intensity of the EAWM (He et al., 2013; Cui and Sun, 1999; Sun and Li, 1997). In the upper troposphere, a key component of the EAWM is the East Asian jet with its maximum core being located to the southeast of Japan (Jhun and Lee, 2004; Boyle and Chen, 1987). Concurrent with the change of these atmospheric circulation, the change of winter surface air temperature (SAT) over East Asia is closely related to the variation in the EAWM (Hao and He, 2017; Lee et al., 2013; Wang et al., 2010).

The EAWM experienced remarkable transitions, with clear weakening since mid-1980s and re-amplification after mid-2000s (e.g., Yun et al., 2018; Wang and Chen 2014). The decadal oscillations in sea surface temperature (SST) are generally considered as the major source of the decadal variability of the EAWM, such as Pacific decadal oscillation and Atlantic multidecadal oscillation (Hao et al., 2017; Ding et al., 2014; Li and Bates, 2007). Jun and Lee (2004) suggested that the Arctic

59 Oscillation may also contribute to the decadal variability in the EAWM. Additionally,

60 above primary components of the EAWM system are subject to obvious changes

61 under the influence of global warming (e.g., Li et al., 2018; Li et al., 2015; IPCC,

62 2013; Hori and Ueda, 2006; Kimoto, 2005; Zhang et al., 1997). Under different global

63 warming scenarios, thermodynamic contrast between the East Asian continent and the

64 Pacific Ocean is reduced uniformly characterized with weakening of the East Asian

65 trough (EAT) as well as the East Asian jet, indicating a weakening of the EAWM (e.g.,

66 Xu et al., 2016; Kimoto, 2005). Previous studies based on Coupled models generally

67 agree on the effect of global warming on the EAWM (Gong et al., 2018; Miao et al.,

68 2018; Hong et al., 2017; Xu et al., 2016; Kimoto, 2005; Hu et al., 2000). Using the

69 phase 5 of the Coupled Models Intercomparison Project output, Miao et al. (2018)

70 deduced that both increased greenhouse gas concentrations and natural forcings

71 (volcanic aerosols and solar variability) play key roles in the interdecadal weakening

72 of the EAWM in the mid-1980s. However, previous studies mainly conduct

73 qualitative research on the potential influence of the global warming, it's still unclear

74 to what extent can the anthropogenic activities impact the EAWM. This study aims to

75 quantitatively estimate the contribution of increasing anthropogenic emissions over

76 the past decades to the change of the EAWM, which is essential for the projection of

77 the EAWM in the future.

78

79 2. Data and Method

80   Monthly mean dataset including SAT, 500 hPa geopotential height and 250 hPa

81 zonal wind is obtained from National Center for Environmental Prediction/National

82 Center for Atmospheric Research (NCEP/NCAR) Reanalysis 1 dataset at a horizontal

83 resolution of $2.5° \times 2.5°$ (Kalnay et al., 1996). Hereafter it is referred to as

84 "observations". To explore the contribution of the anthropogenic emissions to climate

85 change, two different simulations from the C20C+ Detection and Attribution Project

86 (http://portal.nersc.gov/c20c/data.html) are compared in the context of two different

87 forcing scenarios. One is the ***All-Hist*** which was forced with time-vary boundary

conditions (e.g., greenhouse gas concentrations, anthropogenic and natural aerosols, ozone, solar luminosity, land cover, SSTs and sea ice) observed during the past few decades. The other is the ***Nat-Hist*** which was forced with observed SST and sea ice concentrations from which the anthropogenic contribution has been removed (please refer to http://portal.nersc.gov/c20c/data.html for more details). Meanwhile, the natural external forcing such as greenhouse gas concentrations and aerosols was set to preindustrial levels. We analyses the simulations by an atmospheric general circulation model HadGEM3-A-N216 (Christidis et al., 2013; approximately $0.56\,° \times 0.83\,°$ horizontally) available from the C20C+ Detection and Attribution, which has been used to conduct the above two sets of experiments from 1960 to 2013. Both All-Hist and Nat-Hist runs include 15 ensemble members. Each realization in the two scenarios differs from the other only in its initial state. The ensemble-mean of the runs number 1, 2, 5, 13, 14 and 15 (which show a better performance in simulating interannual, decadal and linear trend change of the EAWM) under the All-Hist scenarios agrees best with the reanalysis dataset (such as climatology, interannual and decadal change of the EAWM; evaluation of other runs of model shown in supplementary). Therefore, the simulations of these 6-members ensemble are used in this study.

In this study, we focus on the winter mean which is the average of December, January and February (e.g., the winter 2008 refers to the boreal winter of 2008/2009). Two intensity indices are used to describe the variability of the EAWM: one is defined as the area-averaged height geopotential at 500 hPa in $35\,°$–$45\,°$N, $125\,°$–$145\,°$E (EAWMI_HGT; Sun and Li, 1997); the other is defined as the area-averaged SAT in $25\,°$–$45\,°$N, $105\,°$–$145\,°$E (EAWMI_SAT; Lee et al., 2013). Both area-averaged values are multiplied by -1 so that positive values correspond to strong EAWM; 9-year running mean of the index represents the interdecadal variability of the EAWM.

3. Results and Discussions

3.1 Assessment of the atmospheric circulation pattern simulated by model in All-Hist

117   runs

The EAWM is characterized by northerly winds over East Asia, the Siberian high, the Aleutian low, the deep East Asian trough, the upper tropospheric East Asian jet stream, as well as the cold and dry conditions over East Asia (e.g., Hao et al., 2016; Lee et al., 2013; He and Wang, 2013; Wang and Jiang, 2004; Sun and Li, 1997). In this study, the performance of the HadGEM3-A-N216 model in simulating the above characteristics of the EAWM is firstly evaluated by comparing the corresponding results in the All-Hist runs with reanalysis dataset in the period of 1960–2012.

Figures 1a-d show the climatology of the SAT and 500 hPa geopotential height in winter from the observations and simulations in the All-Hist run. The winter SAT climatology over East Asia in simulations (Fig. 1a) is generally consistent with the observed counterpart (Fig. 1b). The model has successfully reproduced the dominant features of East Asian winter SAT such as the northwest-to-southeast temperature gradient, the 0°C isotherm of SAT stretching from western China (around 27.5 °N) northeastward to north Japan (around 42.5 °N), the cold center located over the Tibetan Plateau (Figs. 1a and 1b). Compared with the observations, the simulated SAT shows apparent cold bias over the north of 40 °N but less bias over the south of 40 °N. In the middle troposphere, the main features (position of axis and intensity) of the EAT are also generally reproduced by the model. The simulated SAT in 25 °–45 °N, 105 °–145 °E (Lee et al., 2013) and 500 hPa geopotential height in 35 °–45 °N, 125 °–145 °E (Sun and Li, 1997) used for the EAWM indices show high spatial correlations with the observations (Fig. 1e), which are exceed 0.99. Additionally, high spatial correlations of the simulated SAT and 500 hPa geopotential height with the observation are accompanied by small root mean square errors (Fig. 1e). It means that the All-Hist runs have well simulated the EAWM climatology.

The variability of the EAWM is also compared between the simulations and the observations. It is found that the correlations between the simulated EAWM indices and the observed EAWM indices are 0.3 for EAWMI_SAT and 0.31 for EAWMI_HGT, respectively (Fig. 2), which are statistically significant. Additionally, the interdecadal variability of the EAWM indices are closely correlated between the

147 simulations and the observation with correlation coefficients of 0.7 for EAWMI_SAT

148 and 0.76 for EAWMI_HGT (Fig. 2). The result suggests that the All-Hist runs have

149 well simulated the interannual and interdecadal variability of the EAWM and can be

150 further used to investigate the anthropogenic impact on the EAWM.

151

152 3.2 Contribution of anthropogenic influence to the East Asian winter monsoon

153 To investigate the anthropogenic contribution to the change of the EAWM, we

154 compare the EAWM in the All-Hist runs with those in the Nat-Hist runs. Both of the

155 EAWM indices in the All-Hist runs show statistically significant decreases over the

156 past decades, with trend coefficients of -0.044 (yr^{-1}) and -0.038 (yr^{-1}), respectively,

157 which are similar to the observed trends (-0.023 and -0.02, respectively; Fig. 2). By

158 contrast, the EAWM indices in Nat-Hist run show an increasing trend, instead (Fig. 2).

159 As shown in Fig. 2, an obviously increasing in EAWMI during 1960-1980 in Nat-Hist

160 runs. The negative phase of Pacific decadal oscillation and Atlantic multidecadal

161 oscillation may be responsible for the enhancing of the EAWM in the Nat-Hist runs

162 during 1960-1980 (Hao et al., 2017; Ding et al., 2014). It suggests that the increasing

163 anthropogenic emissions in the past decades may contribute to the weakening of the

164 EAWM.

165 Figure 3 displays the composited differences of the simulated winter SAT and

166 500 hPa geopotential height between the All-Hist runs and in the Nat-Hist runs, which

167 approximately reflect the response of the EAWM to anthropogenic forcing. The

168 composited differences show clearly that winters with anthropogenic forcing see

169 apparent warmer anomalies over most parts of East Asia except for southeast China as

170 well as warmer conditions over the western North Pacific (Fig. 3a). Such a response is

171 similar to the one revealed by previous CMIP5 studies (Hong et al., 2017; Xu et al.

172 2016). Xu et al. (2016) suggested that the large positive anomalies over high-latitude

173 western North Pacific are due to a north ward shift of the significantly intensified

174 Aleutian low induced by the melting sea ice in the Bering Sea and Okhotsk Sea (Gan

175 et al., 2017). Quantitatively, compared with the situation without anthropogenic

176 influence, the wintertime SAT averaged over (20°–60°N, 100°–140°E) increases by

0.6℃ over the last half-century due to anthropogenic influence (Fig. 3a). At middle troposphere, responses of the 500 hPa geopotential height to anthropogenic forcing shows obviously positive anomalies over East Asia with a value of 15.7 m, implying a shallower EAT which results in less powerful cold air to East Asia (Fig. 3b). The model simulations indicate clearly that the anthropogenic influence may induce a weaker EAWM.

It should be noted that, in the low-level troposphere, the high-latitude warming induced by the anthropogenic forcing is apparently stronger than the warming at lower-latitudes (Fig. 4a), which is the so-called "polar amplification" (Meehl et al., 2007; Collins et al., 2013). Meanwhile, in the high-level troposphere, obviously warming occurs over the tropical regions and the Arctic, but cooling occurs over the high-latitude regions under the anthropogenic influence (Fig. 4a). As a result, a broadening and intensifying Hadley circulation appears, which is consistent with the observed phenomena revealed by previous studies that a poleward expansion and intensification of the winter Hadley circulation in the past few decades (Hu and Fu, 2007; Mitas and Clement, 2005; Hu et al., 2005). Such a change in the Hadley circulation implies a poleward shift of the East Asian jet (Fig. 4b), together with a reinforcement and expansion of Western Pacific subtropical high and a decrease of SLP in the mid-latitude East Asia (Fig. 4c). The change of SLP also indicates a weak decrease of the Siberian high and an intensified Aleutian low. Thus, under the anthropogenic influence, significant easterly anomalies occur in the mid- and high-latitude of East Asia and significant southerly anomalies occur in the low-latitude of East Asia (Fig. 4c), leading to a subdued EAWM. We further explore the contribution of anthropogenic influence to the occurrence of strong/weak EAWM. The case with the normalized index larger than 1.0 (smaller than −1.0) is defined as a strong (weak) EAWM event. The number of the strong/weak EAWM events is shown in Fig. 5. The two observed EAWM indices display 10 (8) and 9 (9) strong (weak) EAWM events during 1960–2012, respectively. Interestingly, the two simulated EAWM indices in the All-Hist run display 11 (10) and 11 (7) strong (weak) EAWM events, respectively. The number of strong or weak EAWM events forced by the

observed time-varying boundary conditions during the past few decades (All-Hist run) is very close to the number in observations. However, during 1960–2012, the simulated two EAWM indices in the Nat-Hist runs display 21 (0) and 19 (0) strong (weak) EAWM events, which is remarkably different from the number in the All-Hist runs as well as the observations. It implies that, in the past decades, the frequency of occurrence of strong EAWM may have reduced by 45% due to the anthropogenic forcing and the anthropogenic forcing is a dominant contributor to the occurrence of weak EAWM.

Note that, there is uncertainty of the EAWM simulated by the Nat-Hist runs. A long-term warming occurred in global SST under the influence of global warming over the past decadal (Fig. 6c), causing a weakened EAWM (Hao et al., 2018). We processed the difference of SST forcing between the All-Hist runs and Nat-Hist runs by empirical orthogonal function analysis as EOF1 (Fig. 6a) and associated principal component 1 (Fig. 6b). The first leading mode shows a long-term oceanic warming with explained variance of 91.4%, characterized by negative anomalies in high-latitude oceans of the southern hemisphere, positive anomalies in tropical oceans and mid-latitude oceans of the southern hemisphere and intense positive anomalies in the high-latitude oceans around 60° N. It shows similar intensity and characteristics to the observed warming over global oceans. However, a cooling occurred in the northern Pacific and an obvious warming over Kuroshio region, which didn't capture by the models, may weaken the EAWM (Sun et al., 2016). This difference may induce an underestimation of the EAWM in Nat-Hist runs.

4 Conclusion

The contribution of the anthropogenic influence to the climatology, trends, and the frequency of occurrence of strong/weak EAWM is explored in this study based on numerical simulations. Firstly, we evaluate the performance of the climate model (HadGEM3-A-N216) in simulating the climatology of wintertime circulation over East Asia and variation of EAWM indices during 1960–2012. The winter-mean states

of SAT and 500 hPa geopotential height related to the EAWM in the All-Hist runs resemble well those in observation with spatial correlation coefficients of greater than 0.99. Also, the interannual and interdecadal variation of the EAWMI_HGT and EAWMI_SAT can be well reproduced by the model under All-Hist scenario. Because of the well performance of the All-His runs in simulating the EAWM indices and winter-mean atmospheric circulation over the East Asia, the exploration about changes of the EAWM induced by anthropogenic influence is considered reliable.

Under All-Hist scenario, the EAWM indices have significantly decline trends over the past decades, which are consistent with those in observations, indicating that the weakening of the EAWM could be simulated by the climate model with all forcing. However, the EAWM indices do not have such trends in the Nat-Hist runs. Compared the area-averaged SAT and 500 hPa geopotential height related to the EAWM for the period of 1960–2012 between two families of experiments, it is found that anthropogenic emissions induce obviously positive SAT anomalies in the most region of East Asia and a weakened EAT, as shown in previous results (Hu et al., 2000; Hori and Ueda, 2006; Xu et al. 2016; Hong et al., 2017; Hong et al., 2017). Additionally, 11 (11) strong EAWM events and 10 (7) weak EAWM events are forced by All-Hist scenario during 1960–2012, which are close to the frequency of occurrence of strong and weak EAWM in observations, while 21 (19) strong EAWM events and 0 (0) weak EAWM event are forced by Nat-Hist scenario. Overall, under anthropogenic influence, during 1960–2012, the EAWM continued to be weakened, and the frequency of occurrence of strong (weak) EAWM had decreased (increased) by 45% (from 0 to 10/7). The poleward expansion and intensification of East Asian jet induced by anthropogenic influence may be the reason for the weakening of the EAWM. A decrease trend is found both in observation and in the All-Hist runs, therefore more attention should be given to the EAWM variability under anthropogenic influence.

Author contributions. Xin Hao conceived the idea for the study and wrote the paper. All authors contributed to the development of the method and to the data analysis.

References:

Boyle, J. S., and Chen, T. J.: Synoptic aspects of the wintertime East Asian monsoon, in: Monsoon Meteorology, edited by: Chang, C. P. and Krishnamurti, T. N., Oxford University Press, 125–160, 1987.

Cui, X. P., and Sun, Z. B.: East Asian winter monsoon index and its variation analysis. J. Nanjing Inst. Meteo., 22, 321–325,1999. (in Chinese)

Chang, C. P., Wang, Z., and Hendong, H.: The Asian winter monsoon, in: The Asian Monsoon, edited by Wang, B., Springer Press, 89–127, 2006.

Christidis, N., Stott, P. A., Scaife, A. A., Arribas, A., Jones, G. S., Copsey, D., Knight, J. R., and Tennant, W.J.: A new HadGEM3-A-based system for attribution of weather- and climate-related extreme events, J. Climate, 26, 2756–2783. doi: 10.1175/JCLI-D-12-00169.1, 2013.

Collins, M., Knutti, R., Arblaster, J., Dufresne, J. L., Fichefet, T., Friedlingstein, P., Gao, X., Gutowski, W. J., Johns, T., Krinner, G., Shongwe, M., Tebaldi, C., Weaver, A. J., and Wehner, M.: Long-term climate change: projections, commitments and irreversibility, In: Climate Change 2013: The Physical Science Basis, Contribution of Working Group I to the Fifth Assessment Report of the Intergovernmental Panel on Climate Change, edited by Stocker, T. F., Qin, D., Plattner, G. K., Tignor, M., Allen, S. K., Boschung, J., Nauels, A., Xia, Y., Bex, V., and Midgley, P. M., Cambridge University Press, Cambridge, UK and New York, NY, 2013.

Ding, Y. H., Liu, Y., Liang S., Ma, X., Zhang, Y., Si, D., Liang, P., Song, Y., and Zhang, J.: Interdecadal variability of the East Asian winter monsoon and its

possible links to global climate change. J. Meteor. Res., 28, 693–713, 2014.

Gan, B. L., Wu, L. X., Jia, F., Li, S. J., Cai, W. J., Nakamura, H., Alexander, M. A., and Milley, A. J.: On the response of the Aleutian Low to Greenhouse Warming, J. Climate,30, 3907–3925. 2017.

Gong, D.Y., Wang, S. W., and Zhu, J. H.: East Asian winter monsoon and Arctic Oscillation. Geophys. Res. Lett., 28, 2073–2076, 2001.

Gong, H. N., Wang L., Zhou W., Chen W., Wu R. G., Liu L., Nath D., and Leung M. Y. T.: Revisiting the northern mode of East Asian winter monsoon variation and its response to global warming. J. Climate, 31, 9001–9014, 2018.

Guo, Q. Y.: Relationship between the variations of East Asian winter monsoon and temperature anomalies in China. Q. J. Appl. Meteorol., 5, 218–225, 1994. (in Chinese)

Hao, X., Li, F., Sun, J. Q., Wang, H. J., and He, S. P.: Assessment of the response of the East Asian winter monsoon to ENSO-like SSTAs in three U.S. CLIVAR Project models. Inter. J. Climatol., 36, 847–866, 2016.

Hao, X., and He, S. P.: Combined effect of ENSO-like and Atlantic Multidecadal Oscillation on the interannual variability of the East Asian winter monsoon. J. Climate, 30, 2697–2716, 2017.

He, S. P., Wang, H. J., and Liu, J.: Changes in the relationship between ENSO and Asia-Pacific midlatitude winter atmospheric circulation, J. Climate, 26, 3377–3393, 2013.

Hao, X., He, S. P., Han, T. T., and Wang, H. J.: Impact of global oceanic warming on winter Eurasian climate. Adv. Atmos. Sci., 35, 1254–1264, 2018.

He, S. P., and Wang, H. J.: Oscillating relationship between the East Asian winter monsoon and ENSO, J. Climate, 26, 9819–9838, 2013.

Hong, J. Y., Ahn, J. B., and Jhun, J. G.: Winter climate changes over East Asian region under RCP scenarios using East Asian winter monsoon indices, Clim. Dyn., 48, 577–595, doi:10.1007/s00382-016-3096-5, 2017.

Hu, Z. Z., Bengtsson, L., and Arpe, K.: Impact of global warming on the Asian winter monsoon in a coupled GCM. J. Geophy. Res., 105, 4607–4624.

326   doi:10.1029/1999JD901031, 2000.

327 Hu, Y., and Fu, Q.: Observed poleward expansion of the Hadley circulation since
328   1979. Atmos. Chem. Phys., 7, 5229–5236, 2007.

329 Hu, Y., Tung, K. K., and Liu, J.: A closer comparison of early and late winter
330   atmospheric trends in the Northern-Hemisphere, J. Climate, 18, 2924–2936,
331   2005.

332 Hori, ME., and Ueda, H.: Impact of global warming on the East Asian winter
333   monsoon as revealed by nine coupled atmosphere ocean GCMs. Geophys. Res.
334   Lett., 33, L03713. doi:10.1029/2005GL024961, 2006.

335 Intergovernmental Panel on Climate Change (IPCC): Climate Change 2013: The
336   Physical Science Basis, Contribution of Working Group I to the Fifth Assessment
337   Report of the Intergovernmental Panel on Climate Change, Stocker, T. F., Qin, D.,
338   Plattner, G. K., Tignor, M., Allen, S. K., Boschung, J., Nauels, A., Xia, Y., Bex,
339   V., and Midgley, P. M., Cambridge University Press, Cambridge, UK, 2013.

340 Jhun, J. G., and Lee, E. J.: A new East Asian winter monsoon index and associated
341   characteristics of the winter monsoon. J. Climate, 17, 711–726, 2004.

342 Jiang, Y., Yang, X. Q., Liu, X., Yang, D., Sun, X., Wang, M., Ding, A., Wang, T., and
343   Fu, C.: Anthropogenic aerosol effects on East Asian winter monsoon: The role of
344   black carbon-induced Tibetan Plateau warming, J. Geophys. Res. Atmos. 122,
345   doi:10.1002/2016JD026237, 2017.

346 Kalnay, E., Kanamitsu, M., Kistler, R., Collins, W., Deaven, D., Gandin, L., Iredell,
347   M., Saha, S., White, G., Woollen, J., Zhu, Y., Chelliah, M., Ebisuzaki, W.,
348   Higgins, W., Janowiak, J., Mo, K. C., Ropelewski, C., Wang, J., Leetmaa, A.,
349   Reynolds, R., Jenne, R., and Josephy, D.: The NCEP/NCAR 40-year reanalysis
350   project, Bull. Amer. Meteorol. Soc., 77, 437–470, 1996.

351 Kimoto, M.: Simulated change of the east Asian circulation under global warming
352   scenario, Geophys. Res. Lett., 32, L16701, doi:10.1029/2005GL023383, 2005.

353 Lau, K. M., and Li, M. T.: The monsoon of East Asia and its global associations-A
354   survey, Bull. Amer. Meteorol. Soc., 65, 114–125, 1984.

355 Lee, S. S., Kim, S. H., Jhun, J. G., Ha, K. J., and Seo, Y. W.: Robust warming over

East Asia during the boreal winter monsoon and its possible causes, Environ. Res. Lett., 8:034001(6pp), 2013.

Li, F., Wang, H. J., and Gao, Y. Q.: Change in sea ice cover is responsible for non-uniform variation in winter temperature over East Asia, Atmos. Ocean. Sci. Lett., 8, 376–382, 2015.

Li, F., and Wang, H. J.: Relationship between Bering sea ice cover and East Asian winter monsoon year-to-year variations, Adv. Atmos. Sci., 30, 48–56, 2013.

Li, Q., Zhang, R. H., and Wang, Y.: Interannual variation of the wintertime fog-haze days across central and eastern China and its relation with East Asian winter monsoon, Int. J. Climatol., 36, 346–354, 2016.

Li, S., He, S. P., Li, F., and Wang, H. J.: Simulated and projected relationship between the East Asian winter monsoon and winter Arctic Oscillation in CMIP5 models, Atmos. Ocean. Sci. Lett., 11, 417–424, 2018.

Li, S. L., and Bates, G. T.: Influence of the Atlantic multidecadal oscillation on the winter climate of East China. Adv. Atmos. Sci., 24, 126–135, 2007.

Meehl, G. A., Stocker, T. F., Collins, W. D., Friedlingstein, P., Gaye, A. T., Gregory, J. M., Kitoh, A., Knutti, R., Murphy, J. M., Noda, A., Raper, S. C. B., Watterson, I. G., Weaver, A. J., and Zhao, Z. C.: Global climate projections, In: Climate Change 2007: The Physical Science Basis, Contribution of Working Group I to the Fourth Assessment Report of the Intergovernmental Panel on Climate Change, edited by Solomon, S., Qin, D., Manning, M., Chen, Z., Marquis, M., Averyt, K. B., Tignor, M., and Miller. H. L., Cambridge University Press, Cambridge, UK and New York, NY, 2007.

Miao, J. P., Wang, T., Wang, H. J., Zhu, Y. L., Sun J. Q.: Interdecadal weakening of the East Asian winter monsoon in the mid-1980s: The roles of external forcings, J. Climate, 31, 8985–9000, 2018.

Mitas, C. M., and Clement, A.: Has the Hadley cell been strengthening in recent decades? Geophys. Res. Lett., 32, L03809, doi:10.1029/2004GL021765, 2005.

Sun, B. M., and Li, C. Y.: Relationship between the disturbances of East Asian trough and tropical convective activities in boreal winter. Chinese Sci. Bull., 42, 500–

504, 1997. (in Chinese)

Wang, B., Wu, Z. W., Chang, C. P., Liu, J., LI, J. P., and Zhou, T. J.: Another Look at interannual-to-interdecadal variations of the East Asian winter monsoon: the northern and southern temperature modes, J. Climate, 23, 1495–1512, 2010.

Wang, H. J., and Jiang, D. B.: A new East Asian winter monsoon intensity index and atmospheric circulation comparison between strong and weak composite. Quaternary Sci., 24, 19–27, 2004. (in Chinese)

Wang, L., Huang, R. H., Gu, L., Chen, W., and Kang, L. H.: Interdecadal Variations of the East Asian winter monsoon and their association with quasi-stationary planetary wave activity, J. Climate, 22, 4860–4872, 2009.

Wang, L., and Chen, W.: The East Asian winter monsoon: Re-amplification in the mid-2000s, Chinese Sci. Bull., 59, 430–436, 2014.

Xu, M. M., Xu, H. M., and Ma, J.: Responses of the East Asian winter monsoon to global warming in CMIP5 models, Int. J. Climatol., 36, 2139–2155, doi:10.1002/joc.4480, 2016.

Yun, J. H., Ha, K. J., and Jo, Y. H.: Interdecadal changes in winter surface air temperature over East Asia and their possible causes, Clim. Dyn., 51, 1375–1390, 2018.

Zhang, Y., Sperber, K. R., Boyle, J. S., Dix, M., Ferranti, L., Kitoh, A., Lau, K. M., Miyakoda, K., Randall, D., Takacs, L., and Wetherald, R.: East Asian winter monsoon: Results from eight AMIP models, Clim. Dyn., 13, 797–820, 1997.

Zhou, W., Chan, C. L. J., Chen, W., Ling, J., Pinto, J. G., and Shao, Y. P.: Synoptic-scale controls of persistent low temperature and icy weather over southern China in January 2008, Mon. Weather Rev., 137, 3978–3991, 2009.

Figure caption:

Figure 1 Climatology of winter-mean (DJF) (a) surface air temperature (shading, ℃) (c) 500 hPa geopotential height (shading, m) during 1960–2012, based on NCEP

reanalysis data. (b), (d) As in (a), (b), but for the model's All-Hist runs. (e) Taylor diagram of winter-mean climatology for surface air temperature (TAS; 25°–45°N, 105°–145°E) and 500 hPa geopotential height (H500; 25°–45°N, 105°–145°E). The rectangle marks the areas used to calculate the climatology in taylor diagram.

Figure 2 (a) The time series of the normalized EAWMI_SAT (curve) and their linear trend (line) during 1960–2012, based on NCEP reanalysis dataset (top), outputs of model in All-Hist run (middle), and outputs of models in Nat-Hist run (bottom). (b) As in (a), but for the EAWMI_HGT. "tr" is an abbreviation for "linear trend coefficient". "∗"means the tr is significant at 95% confidence level based on the Mann-Kendall test, and "′ " means the tr is significant at 90% confidence level. "cor" is an abbreviation for "correlation coefficient between simulated EAWM index under All-Hist scenario and observed EAWM index", "cor_dec" is an abbreviation for "correlation coefficient in decadal time-scale". Note that the time series of the EAWM indices base on outputs of model in the Nat-Hist runs are standardized by the climatology simulated by the All-Hist runs.

Figure 3 Composite differences of winter-mean (a) surface air temperature (shading, ℃) and (b) 500 hPa geopotential height (shading, m) between the All-Hist runs and Nat-Hist runs, during 1960–2012. The plus signs denotes where the composite differences are significant at the 95% confidence level based on two-sided Student t test.

Figure 4 Composite differences of winter-mean (a) air temperature (shading, ℃) over 90°E–150°E, (b) 250 hPa zonal wind (shading, m/s) and (c) sea level pressure (shading, hPa) and 850 wind (vector, m/s) between the All-Hist runs and Nat-Hist runs, during 1960–2012. Red contours denote the climatology of All-Hist runs. The plus signs denotes where the composite differences are significant at the 95% confidence level based on two-sided Student t test.

446

447 Figure 5 (a) The number of strong EAWM events during 1960–2012, based on NCEP

448 reanalysis dataset (left), outputs of model in the All-Hist runs (middle), and

449 outputs of model in the Nat-Hist runs (right). (b) As in (a), but for weak EAWM

450 events.

451 Figure 6 The first leading mode (EOF1; a) and associated principal component (PC1;

452 b) of the difference of the winter-mean sea surface temperature forcing between

453 the All-Hist runs and Nat-Hist runs by empirical orthogonal function analysis

454 based on the period of 1960-2013. The second leading mode (REOF2; c) and

455 associated principal component (RCP2; d) of the winter-mean sea surface

456 temperature from the HadISST data by rotated empirical orthogonal function

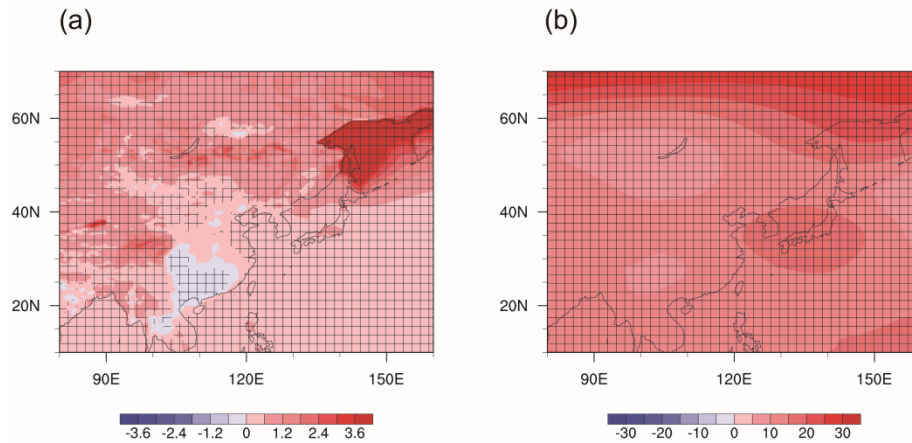457 analysis based on period of 1960-2013.

458

459 Figures
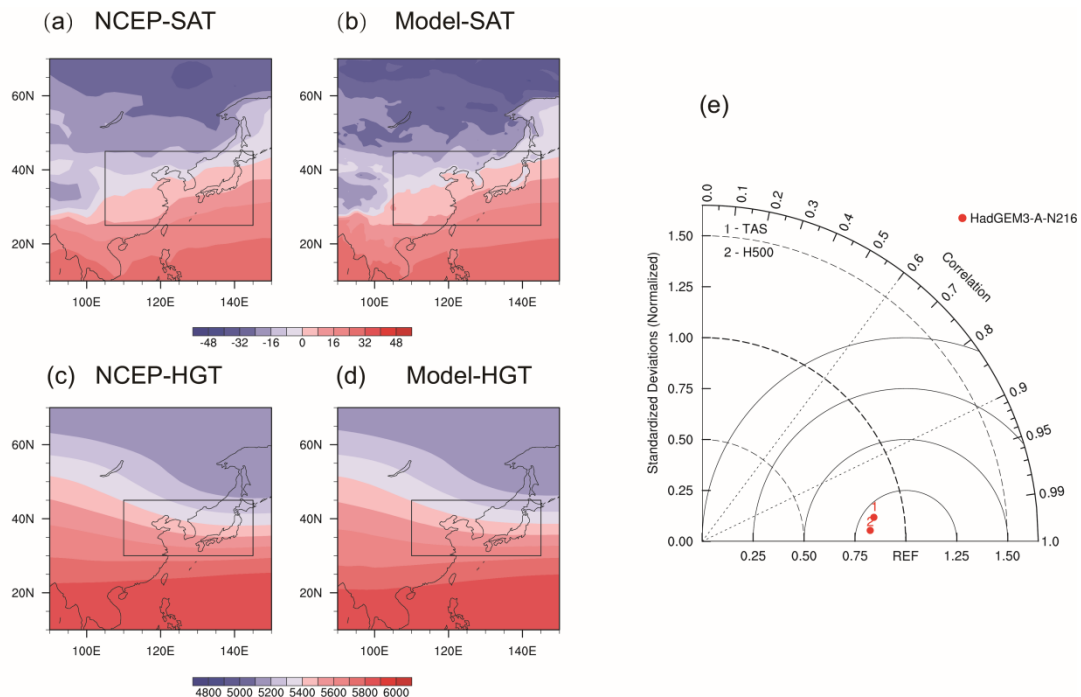
461 Figure 1 Climatology of winter-mean (DJF) (a) surface air temperature (shading, °C)

462 (c) 500 hPa geopotential height (shading, m) during 1960–2012, based on NCEP

463 reanalysis data. (b), (d) As in (a), (c), but for the model's All-Hist runs. (e)

464 Taylor diagram of winter-mean climatology for surface air temperature (TAS;

16

465 25 °–45 °N, 105 °–145 °E) and 500 hPa geopotential height (H500; 25 °–45 °N,

466 105 °–145 °E). The rectangle marks the areas used to calculate the climatology in
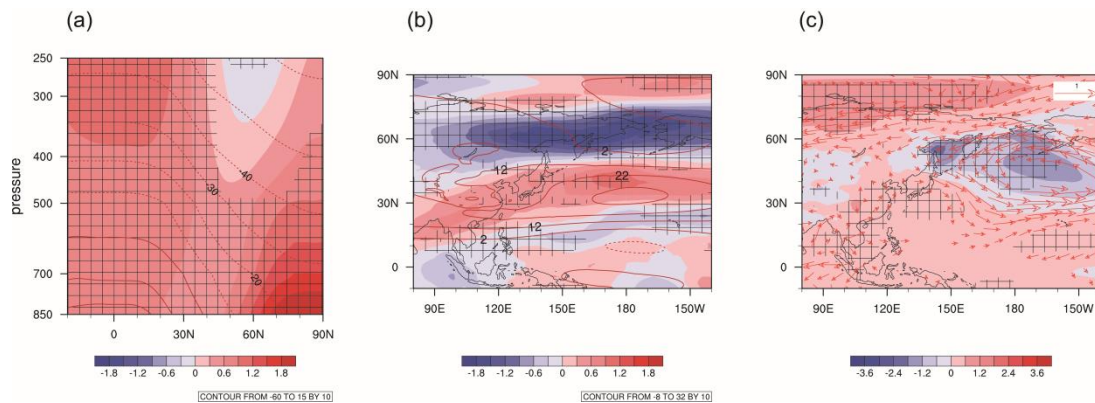
467 taylor diagram.
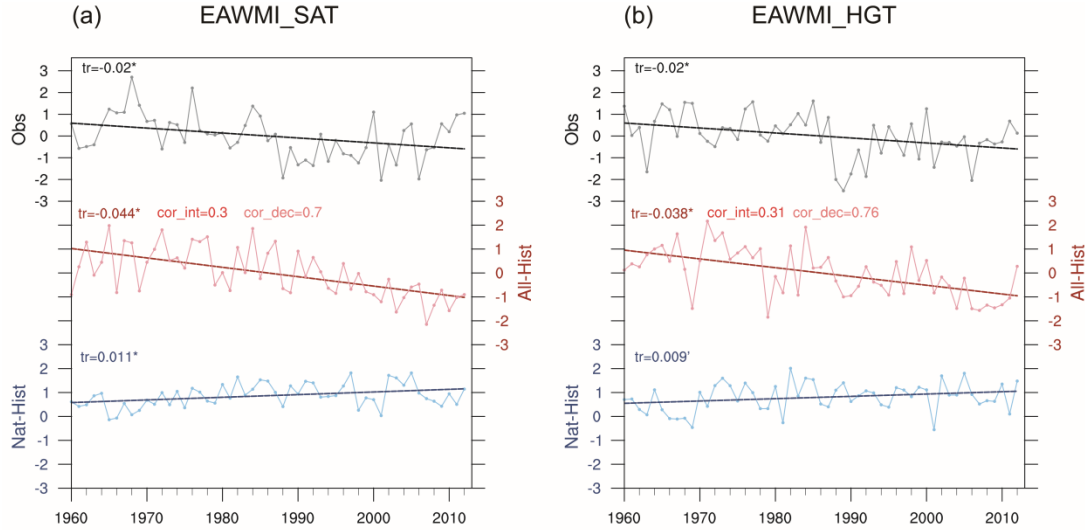
468

469 Figure 2 (a) The time series of the normalized EAWMI_SAT (curve) and their linear

470 trend (line) during 1960–2012, based on NCEP reanalysis dataset (top), outputs

471 of model in All-Hist run (middle), and outputs of models in Nat-Hist run

472 (bottom). (b) As in (a), but for the EAWMI_HGT. "tr" is an abbreviation for

473 "linear trend coefficient". "*"means the tr is significant at 95% confidence level

474 based on the Mann-Kendall test, and "'" means the tr is significant at 90%

475 confidence level. "cor" is an abbreviation for "correlation coefficient between

476 simulated EAWM index under All-Hist scenario and observed EAWM index",

477 "cor_dec" is an abbreviation for "correlation coefficient in decadal time-scale".

478 Note that the time series of the EAWM indices base on outputs of model in the

479 Nat-Hist runs are standardized by the climatology simulated by the All-Hist runs.
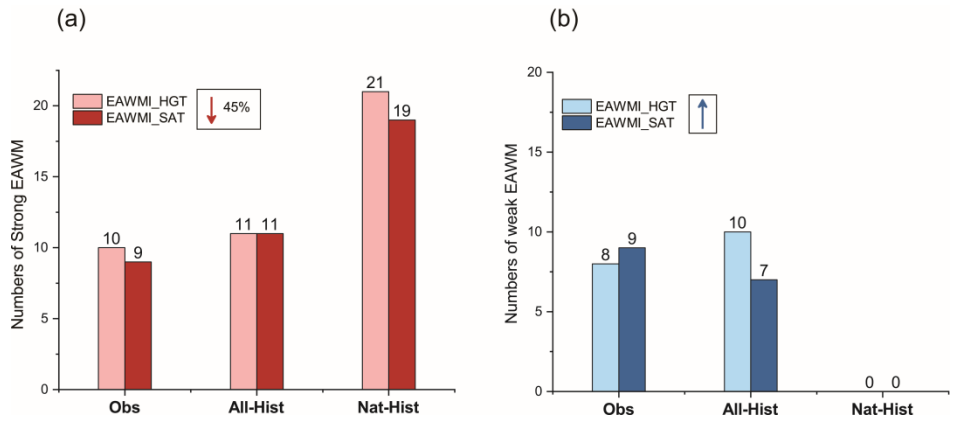
Figure 3 Composite differences of winter-mean (a) surface air temperature (shading, ℃) and (b) 500 hPa geopotential height (shading, m) between the All-Hist runs and Nat-Hist runs, during 1960–2012. The plus signs denotes where the composite differences are significant at the 95% confidence level based on two-sided Student *t* test.


Figure 4 Composite differences of winter-mean (a) air temperature (shading, ℃) over 90 E–150 E, (b) 250 hPa zonal wind (shading, m/s) and (c) sea level pressure (shading, hPa) and 850 wind (vector, m/s) between the All-Hist runs and Nat-Hist runs, during 1960–2012. Red contours denote the climatology of All-Hist runs. The plus signs denotes where the composite differences are significant at the 95% confidence level based on two-sided Student *t* test.

493

Figure 5 (a) The number of strong EAWM events during 1960–2012, based on NCEP reanalysis dataset (left), outputs of model in the All-Hist runs (middle), and outputs of model in the Nat-Hist runs (right). (b) As in (a), but for weak EAWM events.
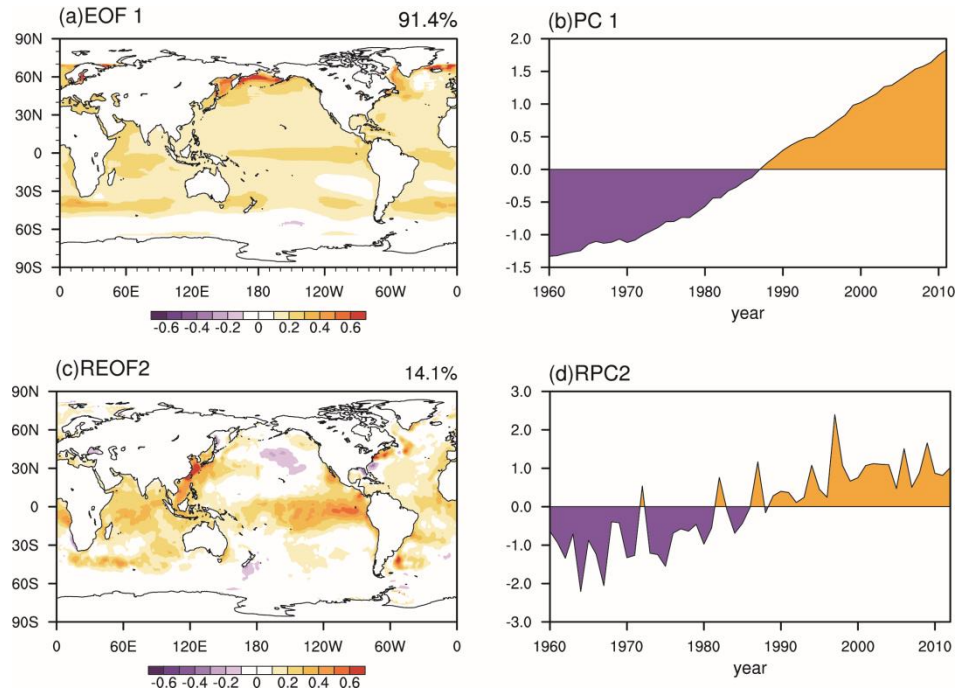
498

Figure 6 The first leading mode (EOF1; a) and associated principal component (PC1; b) of the difference of the winter-mean sea surface temperature forcing between the All-Hist runs and Nat-Hist runs by empirical orthogonal function analysis based on the period of 1960-2013. The second leading mode (REOF2; c) and associated principal component (RCP2; d) of the winter-mean sea surface temperature from the HadISST data by rotated empirical orthogonal function analysis based on period of 1960-2013.

506